Journal of Photochemistry and Photobiology A: Chemistry 221 (2011) 13–21

Contents lists available at ScienceDirect

Journal of Photochemistry and Photobiology A: Chemistry

journal homepage: www.elsevier.com/locate/jphotochem

Elaboration of stable anatase TiO_2 through activated carbon addition with high photocatalytic activity under visible light

Houda Slimen[a,*], Ammar Houas[a], Jean Philippe Nogier[b]

[a] Equipe de Catalyse et Environnement, URECAP ENIG/Faculté des Sciences de Gabès Université de Gabès Campus Universitaire, 6072 Gabès, Tunisia
[b] Laboratoire des Systèmes Interfaciaux à l'Echelle Nanométrique (S.I.E.N) Université P. et M. Curie Paris VI 4 place Jussieu case 196, - tour 54, 75252 Paris Cedex 05, France

ARTICLE INFO

Article history:
Received 4 December 2010
Received in revised form 21 February 2011
Accepted 11 April 2011
Available online 16 April 2011

Keywords:
TiO_2
Activated carbon
Sol–gel
Degradation
Visible irradiation

ABSTRACT

Photoactive TiO_2 was directly obtained by sol–gel method or from titanium dioxide/activated carbon composite (TiO_2/AC), then calcinated under air at 700 °C. The obtained materials were characterized by N_2 adsorption (77 K), X-ray diffraction (XRD), diffuse reflectance UV-vis spectroscopy (UV/DRS) and transmission electron microscopy (TEM). The solid prepared from (TiO_2/AC) composite was found to be mainly pure anatase phase with SiO_2 and Fe_2O_3 traces, whereas, pure TiO_2 was predominantly rutile. Adding activated carbon increases the surface area of photocatalyst, reduces the grain size of titania particles and causes a blue shift of the light absorption spectrum due to the quantization of band structure. Photocatalytic activity was tested and compared with that of TiO_2 Degussa P25 on the degradation of methylene blue (MB) in an aqueous solution under visible irradiation. TiO_2(AC-700) catalyst was found to be two times more active than TiO_2-P25.

1. Introduction

Heterogeneous photocatalysis research has received great interest in the two last decades, especially for the purification of wastewater [1–6]. Even if the famous titanium dioxide (TiO_2) semiconductor is the most used, because of its photocatalytic activity, high stability, non-toxicity and inexpensiveness, the interest is much more focused nowadays on the synthesis of photocatalyst materials to overcome some limitations of the use of TiO_2. Some of the important limitations are: TiO_2 powder is difficult to recycle, easy to agglomerate, and causes a problem of separation from the solution [7]. Furthermore, TiO_2 is a wide band-gap semiconductor (3.20 eV for anatase TiO_2 and 3.02 eV for rutile TiO_2) which makes the photocatalytic activity quite limited in the visible light, solar and fluorescent light [8].

For these reasons and others, several approaches have been followed, even if the way to enhance the photocatalytic efficiency is still a critical concern. Some of these approaches are: (i) preparing new photocatalysts based on metals oxides other than TiO_2 [9–11] (ii) doping and/or codoping TiO_2 [12–14] (iii) immobilizing TiO_2 on an inert and suitable supporting matrix [15–18] in order to increase the active area as a promising pathway to enhance the photodegradation of pollutant molecules in vapor- or liquid-phase [19,20]. For this purpose several porous media are used, as far as possible, to provide a vast pore structure for dispersing TiO_2 photocatalysts such as zeolite, alumina, silica, glass, carbon nanotube and activated carbon [21–26].

Among these materials, activated carbon (AC) is widely used as a support in gas and water remediation due to its good adsorption properties and seems to be an attractive support for TiO_2 [27–29]. Indeed, a synergistic effect has been already observed by using TiO_2 and AC as mechanical mixture or composite [30,31].

The temperature and atmosphere of calcination of the TiO_2/AC precursor have a very important effect on the properties and activity of the final TiO_2/AC composite. Unfortunately, many researchers do not always specify the atmosphere of calcination of the TiO_2/AC precursor. When calcinations took place under inert atmosphere, the surface area would increase implying that an enhancement in the TiO_2/AC activity may due especially to the synergistic effect between AC and TiO_2. Moreover, the activity was limited under visible light due to the total absorption of the light by the activated carbon. But when the calcination took place under air or oxygen atmosphere, the total combustion of activated carbon could be expected beyond 400 °C. In this case, a significant decrease of the surface area is observed and the synergistic effect due to the presence of common contact interface created between both solids must disappear.

Many oxides from metals inorganic species (such as Fe, Ca, Mg, Na, K, Si, Al, V and Ni) are usually present in the basic matrix of activated carbon. Certain transition group metals contributed to the oxidation reactions as catalysts [32]. In this work, a sol–gel method was used to prepare a bare TiO_2 photocatalyst and TiO_2

* Corresponding author. Tel.: +216 75 39 26 00; fax: +216 75 39 24 21.
E-mail address: houda_slim@yahoo.fr (H. Slimen).

1010-6030/$ – see front matter © 2011 Elsevier B.V. All rights reserved.
doi:10.1016/j.jphotochem.2011.04.013

through activated carbon addition. Since the calcination was carried out under air at high temperature (700 °C), we expected the AC disappearance but we wanted to check and confirm that the activated carbon was not acting only by synergistic effects to increase the adsorption and promote contact pollutant photocatalyst. Many experiments were conducted to understand how the presence of AC influences the physico-chemical properties of the photocatalyst: is it only an increase in contact area? Or does it completely change the structural and textural properties of TiO_2? Do the oxides present in AC ash, such as SiO_2, Fe_2O_3, Al_2O_3, Na_2O, CuO and K_2O... [33] have any effects?

For this purpose, we investigated the physicochemical properties of the prepared photocatalyst TiO_2(AC-700) by X-ray diffraction, BET analysis, UV-vis spectroscopy and transmission electron microscopy (TEM). Methylene blue was selected to evaluate the photocatalytic activity of TiO_2(AC-700) under visible light. Such molecule is usually used as representative of dyes commonly discharged in wastewater.

2. Experimental

2.1. Synthesis of bare TiO_2 and TiO_2(AC-700) photocatalysts

TiO_2 was prepared directly by titanium tetraisopropoxide hydrolysis (TTIP ($Ti(OC_3H_7)_4$) Fluka pure grade), 0.067 mol of TTIP was dissolved in 10 ml isopropanol (Fluka). After stirring for 5 min at room temperature, 30 ml water was added dropwise. The solution was maintained under stirring for 60 min until a homogenous gel was formed. The activated carbon used for the composite preparation was CECA 12-40 (Calgon Carbon Corporation). The TiO_2/AC catalyst was prepared by a similar method by adding 2.67 g of activated carbon (50 wt.% with regard to the TiO_2 amount) to the TTIP-iPrOH solution. The gels were dried at 100 °C for 12 h. The obtained solids were ground and calcinated at 700 °C in air flow for 2 h to obtain bare TiO_2 and TiO_2(AC-700) samples.

2.2. Photocatalysts characterization

X-ray diffraction patterns were recorded using a PANalytical X-ray diffractometer in the range $2\theta = 10–100°$ using CuKα as X-rays source and the average crystallite size of anatase and rutile phase were determined according to the Scherrer equation using the full width at half maxima (FWHM) of the main peak of each phase.

The BET surface area and pore size distribution were determined by N_2 physisorption at 77 K using a Micrometrics 2010 apparatus. Before the adsorption test, the samples were out-gassed at 200 °C until the residual pressure decreases below 3 μmHg. BET surface area was determined by multipoint BET method using the adsorption data in the relative pressure (P/P_0) range of 0.05–0.25. Desorption isotherms were used to determine the pore size distribution using the Barret–Joyner–Halander (BJH) method with cylindrical pore size.

TEM measurements were performed on a Philips G20 Ultra-Twin transmission electron microscope equipped with a CCD camera. Operating at 200 kV, the microscope reaches a point resolution of 0.14 nm and a line resolution of 0.1 nm. Scale calibration was done on the Au (1 0 0) planes. Both dry and wet depositions were performed with ethanol and water as solvent. Powders were deposited on carbon coated copper grids.

For the characterization of the light absorption features and band-gap determinations, diffuse reflectance spectra (DRS) of the powders were measured in the range of 200–800 nm on a UV-Vis-NIR scanning spectrophotometer (Shimadzu, 3101 PC) equipped with an integral sphere using $BaSO_4$ as a reference. The photocatalyst powder was placed in the sample holder on an integrated sphere for the reflectance measurements.

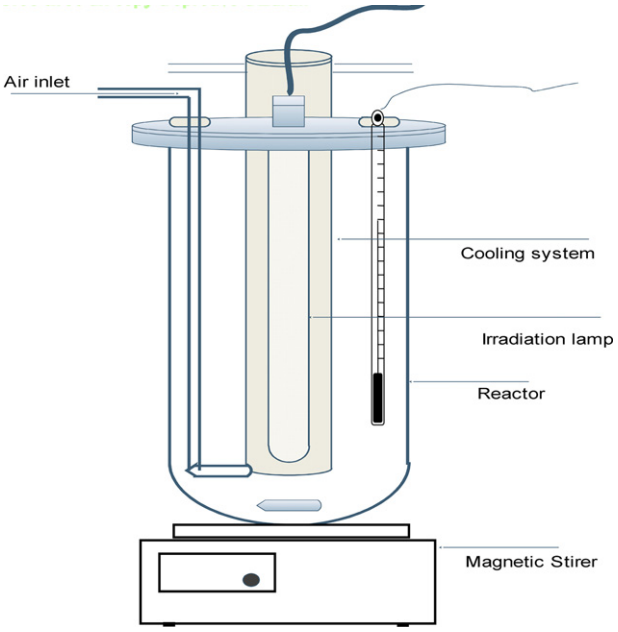

Fig. 1. Schematic diagram of the static photocatalytic reactor.

2.3. Photoreactor and photodegradation experiments

The experiments were carried out using a cylindrical batch reactor (Fig. 1) opened at the air with 150 ml of capacity. The visible irradiation source was a commercial Halogen lamp (Duralamp 250 W). The lamp was maintained in the centre of the reactor and placed in an axial position inside the water jacket crossed by the water circulation to avoid heating of the solution. The UV emission of the lamp is filtered to approximate to sunlight while avoiding its variation with time and cloudiness. The relative emitted light intensity of the lamp was obtained (Fig. 2) by using radiometric calibration standard (Ocean Optics) and the intensity of light is about 140 W/m^2.

Methylene blue MB (Aldrich) was chosen as a model molecule for the photocatalytic test. Such molecule is usually used as representative of dyes commonly discharged in wastewater. For all experiments, the reactor was initially loaded with 125 ml MB

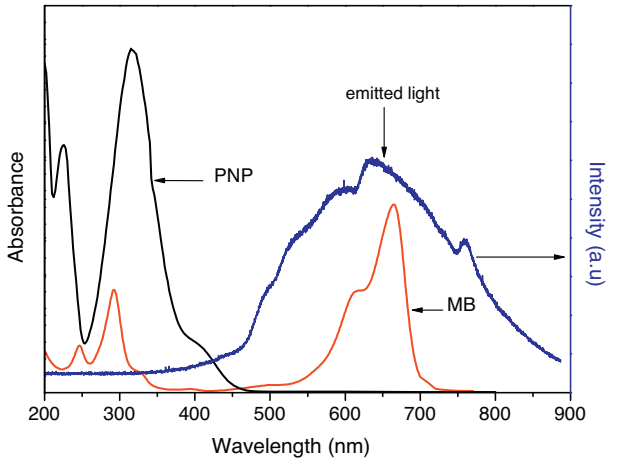

Fig. 2. UV–vis absorption spectrum of MB, PNP aqueous solution and the relative emitted light intensity of the lamp.

aqueous solution (30 mg/l) and 0.5 g/l of catalyst, the mixture maintained in a continuous stirring. Before the illumination, the suspension was stirred in the dark for 90 min to establish the adsorption–desorption equilibrium. 2 ml of suspension was withdrawn periodically and immediately centrifuged at 8000 rpm for 15 min to separate the catalyst from the solution. 1 ml was diluted five times and its absorbance at 664 nm was measured by UV-Vis spectroscopy (Shimadzu spectrophotometer UV-1700). Total organic carbon (TOC) was determined by using a TOC-V_e Analyzer (Shimadzu) to follow the mineralization of MB.

3. Results and discussion

3.1. Catalysts characterization

3.1.1. X-ray diffraction analysis

The X-ray diffraction (XRD) patterns of activated carbon, bare TiO_2 and TiO_2(AC-700) are shown in Fig. 3. The TiO_2 phase composition was calculated from the integrated intensities of anatase (1 0 1) and rutile (1 1 0) peaks using the following formulas. Eq. (A.1) [34]

$$W_A = \frac{k_A A_A}{(k_A A_A + A_R)} \quad \text{and} \quad W_R = \frac{A_R}{(k_A A_A + A_R)} \tag{A.1}$$

W_A and W_R represent the weight fractions of anatase and rutile, respectively. A_A and A_R are the integrated intensities of anatase (1 0 1) and rutile (1 1 0) peaks, respectively while k_A is a constant equal to 0.886. The crystal size of the particles was determined using the Scherrer formula. Eq. (A.2)

$$L_{hkl} = \frac{k\lambda}{\beta \cos\theta_{hkl}} \tag{A.2}$$

where L_{hkl} is the crystalline size in nm, λ (0.15418 nm) is the wavelength of the X-ray radiation, k usually taken as 0.89 and β is the line width at half maximum height for the anatase (1 0 1) peak ($2\theta = 25.37^\circ$) and for the rutile (1 1 0) peak ($2\theta = 27.62^\circ$).

The XRD pattern of activated carbon corresponds to that of amorphous carbon containing different mineral species, mainly SiO_2 and Fe_2O_3 [33,35].

The XRD pattern of bare TiO_2 show that the catalyst contains 10% of anatase and 90% of rutile phase, while the TiO_2(AC-700) is mainly constituted by anatase phase with trace of SiO_2. The disappearance of Fe_2O_3 phase was observed. The persistence of only SiO_2 oxide is probably due to its major quantities in the activated carbon. The stability of anatase phase leads to conclude that the activated carbon suppresses the phase transformation of titania anatase to rutile. AC matrix with high surface areas baffles the anatase to rutile phase transformation resulting from its large interfacial energy, which creates the anti-calcination effects for AC matrix [36–38].

The crystallite size of TiO_2 and TiO_2(AC-700) samples were calculated to be, respectively 60 and 17 nm. The addition of activated carbon to TTIP-iPrOH solution during TiO_2 elaboration may be responsible of this crystallite size reduction by the fact that the formation of TiO_2 can occurs into the pores of activated carbon. Moreover, the presence of SiO_2 and Fe_2O_3 oxides in AC matrix may inhibit grain growth by providing a barrier among titania grains [32].

3.1.2. Optical features

The DRS spectra of TiO_2 and TiO_2(AC-700) samples are shown in Fig. 4(a). A blue shift in the UV-visible spectrum towards the lower wavelength side was observed in TiO_2(AC-700) sample. At the same time, the absorption clearly increase for TiO_2(AC-700) in the UV region but slightly in the visible region compared to bare TiO_2 extending its activity under visible irradiation. To calculate the band gap energies, DRS experimental data were converted to

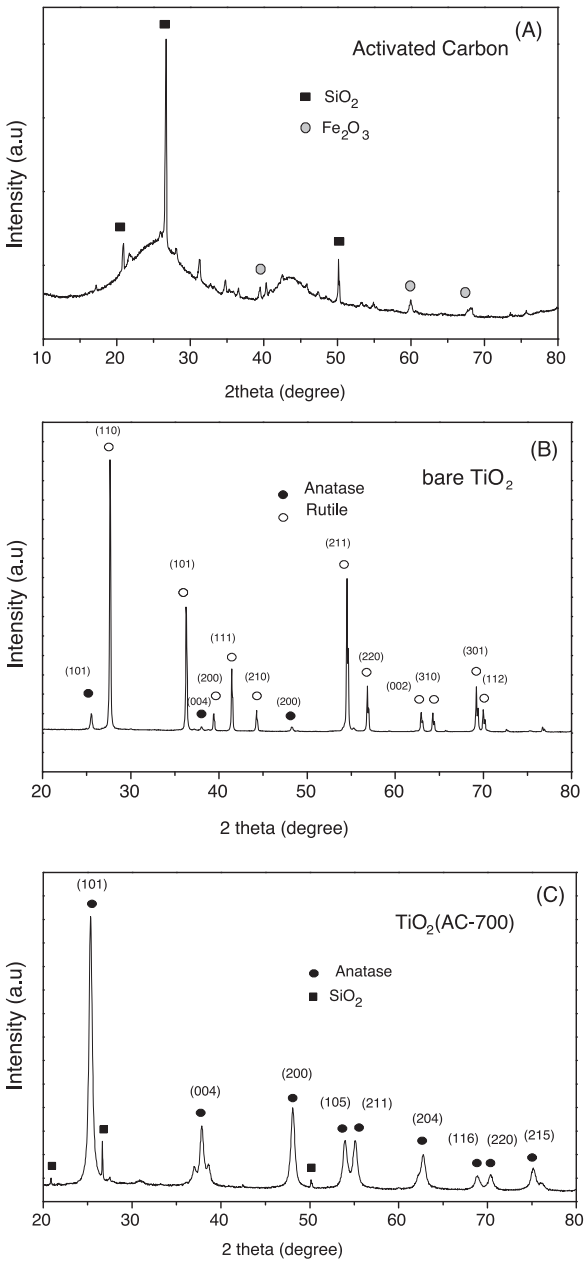

Fig. 3. XRD patterns for the activated carbon (A), bare TiO_2 (B) and TiO_2(AC-700) (C).

absorption coefficient values $F(R)$ according to the Kubelka–Munk equation [39,40] Eq. (A.3):

$$F(R_\infty) = \frac{(1 - R_\infty)^2}{2R_\infty} \tag{A.3}$$

$F(R_\infty)$ is the so-called remission or Kubelka–Munk function where ($R_\infty = R_{sample}/R_{standard}$).

The theory of interband optical absorption shows that at the absorption edge, the absorption coefficient of a semiconductor can be expressed as:

$$[F(R_\infty)h\nu]^n = A(h\nu - Eg) \tag{A.4}$$

where h is the Planck's constant (6.62608×10^{-34} J s), ν is the frequency of the light (s^{-1}), A is a constant, Eg the band-gap of allowed transitions (eV), and n is a number characterizing the transition process. For an indirect TiO_2 allowed transition, n is equal to 0.5. Therefore, a transformed Kubelka–Munk function can be con-

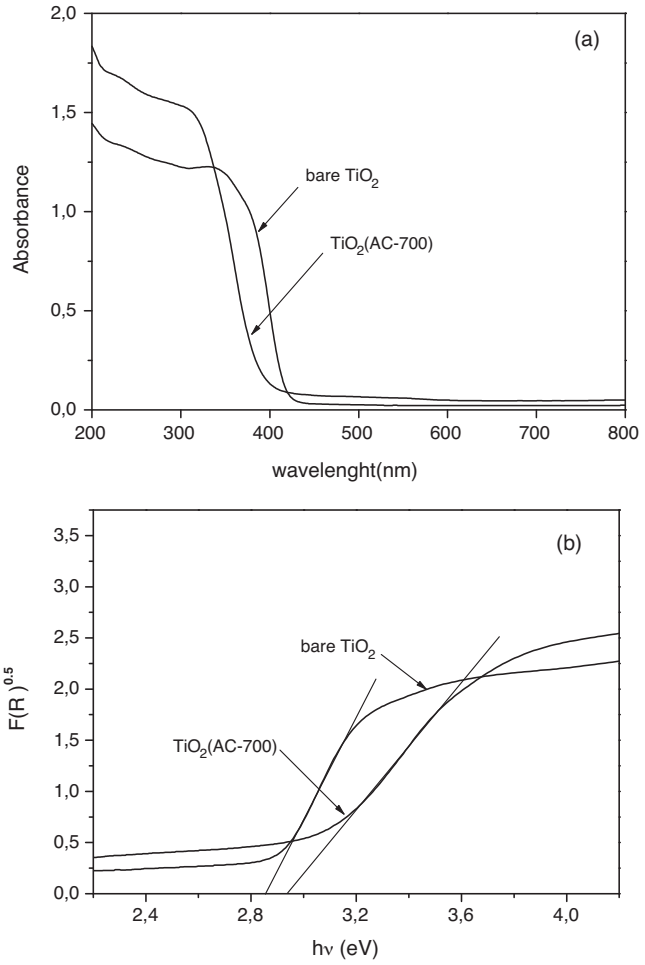

Fig. 4. (a) Diffuse reflectance UV–vis spectra for bare TiO_2 and TiO_2/AC; (b) Kubelka-Munk elaboration.

structed by plotting $[F(R_\infty)]^{0.5}$ against $h\nu$ to obtain the band gap of the TiO_2 particles [41]. To obtain the band gap value, the converted curves can be fitted by a Boltzmann sigmoidal equation. As showed in Fig. 4(b), the x-axis intercept of the line tangent to the inflection point of the curve provides the band gap values as 2.94 and 2.85 eV for TiO_2(AC-700) and TiO_2, respectively.

The observed blue shift and the increased band gap indicate that the band structure of TiO_2(AC-700) becomes quantized. This result is in good agreement with the decrease of particle size (from 60 nm to 17 nm) and the anatase phase content. The quantization in the band structure of TiO_2(AC-700) may improve the photoactivity since the electrons photoexcited are confined in the conduction band and their life time is elongated. Thus, the electron hole recombination rate during the illumination of catalyst decreases [42–44]. As a result, the photocatalytic activity is supposed to be improved. Furthermore, the increase of the band gap energy can be attributed to the interface interaction due to the presence of SiO_2 oxides in the catalyst. This effect was also seen by Periyat et al. [32].

3.1.3. Morphological characterization

Fig. 5(a)–(c) shows the N_2 adsorption–desorption isotherms of activated carbon, bare TiO_2 and TiO_2(AC-700) composites, respectively. The typical isotherm type II is identified for both activated carbon and TiO_2. The hysteresis loop H_4 type was observed with activated carbon and it was indicative of its microporosity and confirms the existence of the narrow slit-like pores usually associated to activated carbon.

Table 1
Textural characterization results for activated carbon (AC), synthesized bare TiO_2 and TiO_2(AC-700) photocatalysts and anatase rutile repartition.

Parameters	AC	Bare TiO_2	TiO_2(AC-700)
S_{BET} ($m^2\,g^{-1}$)	1058	5.8	51.5
V pores total ($ml\,g^{-1}$)	0.68	0.01	0.13
L_{hkl} (nm)	–	60	17
Anatase (%)	–	10	100

The TiO_2 isotherm presents a hysteresis loop H_3 type suggesting the presence of aggregate particles which can be assigned to a capillary condensation taking place in non rigid texture.

The typical isotherm type IV is observed in the case of the synthesized TiO_2(AC-700). The mesoporosity of this sample is confirmed by the hysteresis loop H_2 type. We can observe that the adsorption at lower P/P_0 increases from bare TiO_2 to TiO_2(AC-700) to activated carbon, which is in correlation with the S_{BET} values obtained (Table 1). Both TiO_2(AC-700) surface area and pore volume are ten times higher than that of bare TiO_2. Since calcinations occurred at high temperature (700 °C) in flow of air, normally, activated carbon is totally transformed to ash. Oxides present in ash content of activated carbon, such as silica, can enter the matrix which could increase the defects in the titania matrix and therefore the surface area would increase [32].

Fig. 6(a and b) shows TEM images of the surface of bare TiO_2 and TiO_2(AC-700) powders respectively. Only one type of morphologies was observed: spherical-like TiO_2 particles. We note and confirm the absence of the AC matrix in the final TiO_2(AC-700) powder by the fact that after calcinations the activated carbon was completely burned giving rise to white colors photocatalyst.

Furthermore, the particles size of the bare TiO_2 powders is greater than that of TiO_2(AC-700) suggesting that in absence of AC, the TiO_2 powder agglomerate more easily during the calcinations process. AC matrix acted as a barrier which controlled the growth of TiO_2 particles and prevents their agglomeration which has been also reported by Li et al. [36] and Wang et al. [37]. Furthermore, these effects can be related in part with the decrease in the particle size observed previously by XRD in the case of TiO_2(AC-700), but possibly also with the progressive occurrence of sintering phenomena, leading to larger aggregates of TiO_2 in absence of activated carbon. Moreover, the decrease in particle size can be correlated with the observed increase of the surface area (approximately ten times higher for TiO_2(AC-700) than for bare TiO_2).

Fig. 6(c and d) shows the spectra taken using Energy Dispersive X-ray (EDX) for both photocatalysts and the corresponding data were listed in tables included. These spectra showed that the main elements presents are Ti and O in the ration 1:2 and no C was detected. However in the case of the TiO_2(AC-700) sample, the presence of Si element was confirmed which is in correlation with the XRD results but the values of the elements weight percents can not be explained in this level.

3.2. Photocatalytic performance

3.2.1. Adsorption kinetic studies

The adsorption phenomena over TiO_2-P25, bare-TiO_2 and TiO_2(AC-700) were studied in the dark for initial concentration of MB equal to 30 $mg\,l^{-1}$ and 0.5 $g\,l^{-1}$ of catalyst concentration. The pH was maintained constant and it was the initial pH (6.7) of the MB solution. All experiments were carried out with the same agitation speed.

Adsorption kinetics obtained and shown in Fig. 7 indicate that the thermodynamic equilibrium time was 60 min. To study the kinetics of adsorption in its totality, the Lagergren model [45] given

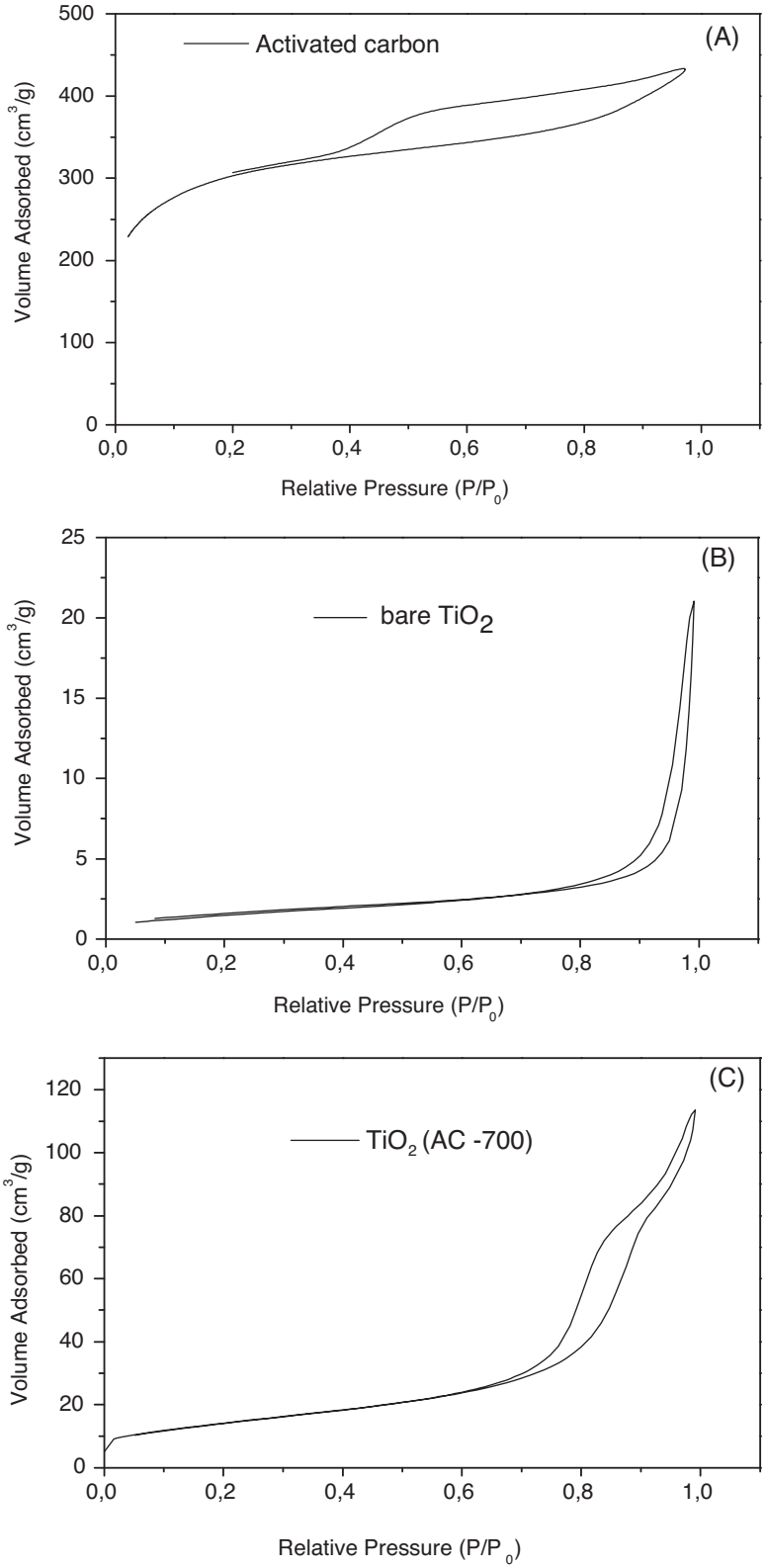

Fig. 5. N_2 adsorption isotherms of (A) activated Carbon, (B) bare TiO_2 and (C) TiO_2(AC-700).

by the following equation was used. Eq. (A.5):

$$q_t = q_e\,[1 - \exp(-k_{ads}t)] \quad (A.5)$$

where q_t and q_e (mg g^{-1}) are the adsorbed amount at t instant and at equilibrium respectively, k_{ads} is the apparent kinetic constant (min^{-1}). The adsorption kinetics was well fitted as first order with this model. The Lagergren parameters obtained q_e, k_{ads} and the correlation coefficient are given in Table 2. The presence of activated carbon enhance both MB equilibrium adsorbed amount and the apparent constant k_{ads} which can be correlated with the increase

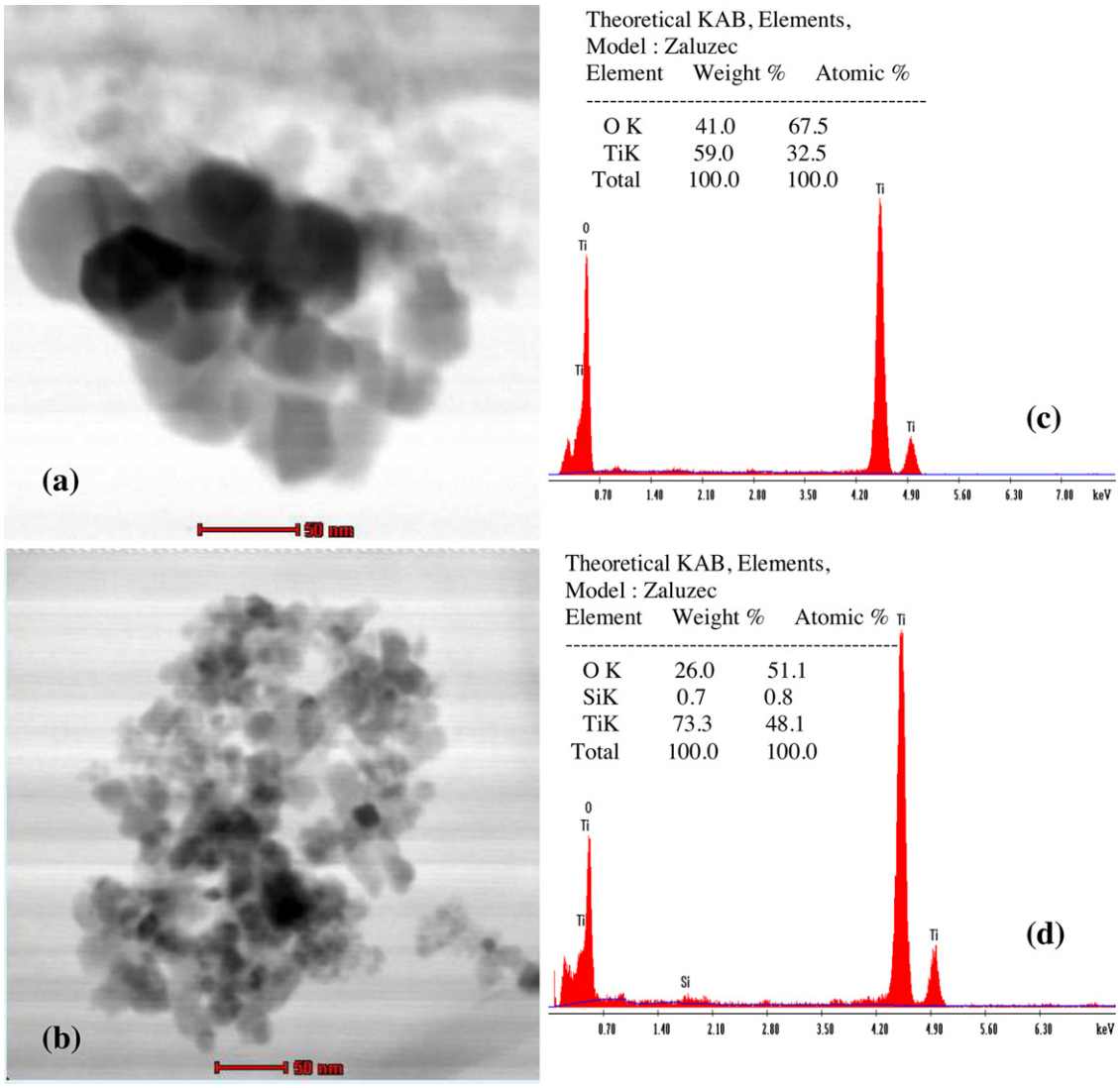

Fig. 6. TEM micrographs and EDX spectra of (a) and (c) bare TiO_2; (b) and (d) TiO_2(AC-700).

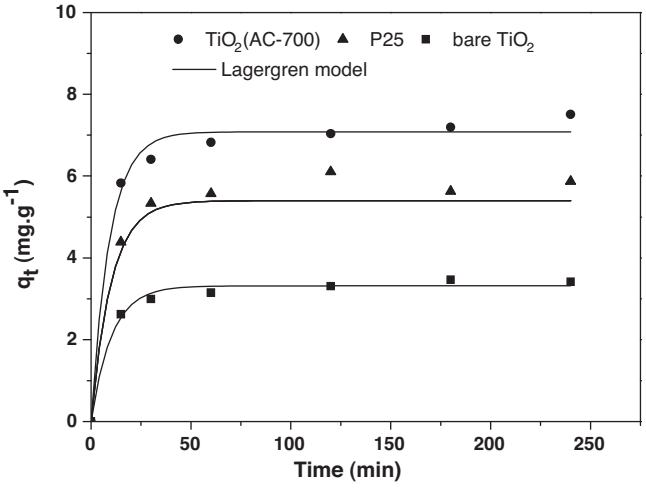

Fig. 7. Adsorption kinetics of methylene blue in the dark on TiO_2-P25, bare TiO_2 and TiO_2(AC-700).

of surface area and total pore volume of TiO_2 as already mentioned. Moreover, TiO_2(AC-700) catalyst exhibit the high BET surface area which may provides more active sites for the photocatalytic reaction

3.2.2. Photocatalytic degradation

The photocatalytic activity of TiO_2(AC-700) and bare TiO_2 materials were evaluated by using the degradation of the standard organic dye, methylene blue (MB), under visible light irradiation as probe reaction. For comparison, the activity of the commercial photocatalyst TiO_2 Degussa P25 and synthesized photocatalysts were tested under the same conditions.

The results displayed in Fig. 8 show that MB solution becomes completely decolorized within 180 min of irradiation with TiO_2(AC-

Table 2
Kinetic parameters of methylene blue adsorption on the dark and degradation under visible irradiation on TiO_2-P25, bare TiO_2 and TiO_2(AC-700) photocatalysts.

Sample	Dark adsorption			Visible light degradation	
	q_e (mg g^{-1})	k_{ads} (10^{-2} min^{-1})	r^2	k_{app}(10^{-3} min^{-1})	r^2
TiO_2(AC-700)	7.88	10.12	0.98	49.75	0.99
Bare TiO_2	3.32	9.16	0.98	18.58	0.99
TiO_2 P25	5.39	9.90	0.97	22.74	0.99

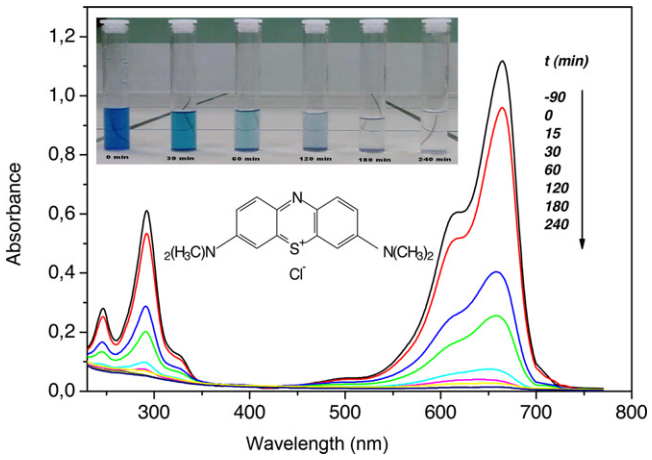

Fig. 8. Changes in the UV–vis spectra during photodegradation of methylene blue on TiO_2(AC-700) (inset: molecular structure of MB).

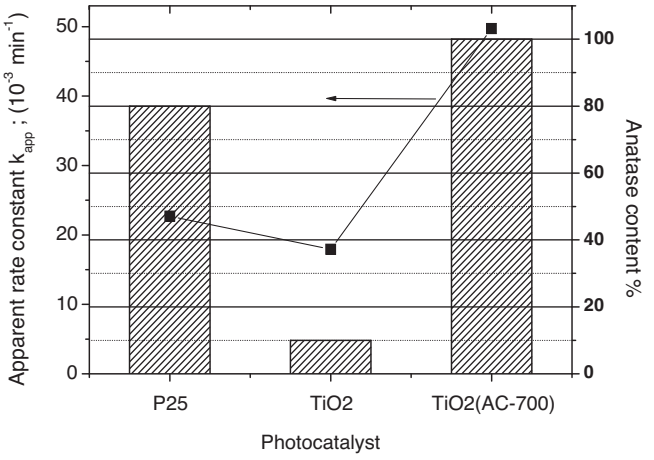

Fig. 10. Apparent rate constants of MB for the photocatalytic degradation as a function of catalysts and correlation with anatase phase ratio.

700) sample. This figure shows also, the UV–vis absorption spectra of MB which were studied at different times of irradiation. As it is presented, the bands relating to different molecular parts in this dye are decreased with respect to time. MB is a phenothiazine dye in which the chromophore part of molecular structure contains amino and thiocarbonyl linkage and shows a strong absorbance in the visible region, while the absorbance peaks of the benzene rings appear in the UV region. The perfect disappearance of the bands at 664 nm and at 290 nm reveals that MB is eliminated in the presence of TiO_2(AC-700) suspension.

Normalized kinetics of MB degradation in presence of visible light with and without catalysts are shown in Fig. 9. In all the cases these kinetics are well fitted with a classic first order given by the following equation Eq. (A.6)

$$C_t = C_0 \exp(-k_{app} t) \quad \text{(A.6)}$$

where C_0 is the initial MB concentration, C_t is its concentration at t time and k_{app} is the apparent first order constant. Total removal of MB can be obtained in the case of TiO_2(AC-700) after less than 150 min while it needs more than 200 min with the other photocatalysts tested. The total mineralization of methylene blue using TiO_2(AC-700) was also improved by measuring the TOC before irradiation (15.80 ppm) and after 180 min of irradiation and it was found to be equal to 2 ppm. Results show also that direct photolysis of MB solutions without catalyst followed pseudo first-order kinetics with an apparent rate constant equal to 0.006 min^{-1}.

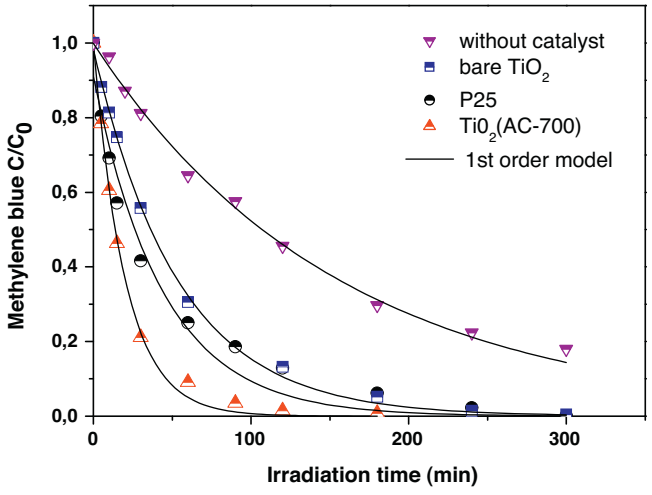

Fig. 9. Photocatalytic degradation of MB in aqueous suspension as a function of visible irradiation time with bare TiO_2, TiO_2-Degussa P25 and TiO_2(AC-700). Experimental condition: natural pH; C_0(MB) = 30 ppm; m (catalyst) = 62.5 mg; V (solution) = 125 ml.

All apparent rate constant k_{app} for the different photocatalysts are summarized in Table 2. A correlation between anatase amount in catalyst and its apparent rate constant was found and shown in Fig. 10. The apparent rate constant of TiO_2(AC-700) is much higher than those of TiO_2-P25 and bare TiO_2. In presence of dye and visible light the photoactivity of catalyst must be demonstrated.

Many researches [46–48] have proposed that photocatalytic process and photosensitized process contributed together in the degradation of dye by TiO_2 especially in the presence of visible irradiation. In our experiments, the degradation of methylene blue is performed by the means of three processes: the direct photolysis, the photosensitized process and the photocatalysis.

Through the interaction of visible light and methylene blue, which characterized by a main band at 664 nm and exhibit high absorption of the visible light emitted by the lamp (Fig. 2), three possible ways can be presented in the mechanism of degradation of MB in absence of catalyst. The first way passes through a cationic radical, while the others involve either oxygen or hydroxyl radical. For each of these pathways, the first step is the absorption of photon by MB with energy at least equal to the difference energy between the highest occupied orbital (HOMO) and the lowest unoccupied orbital (LUMO), leads to the excited state of MB (Eq. (1)). This last excited state can return to its original state when it reacts with the dissolved oxygen, or generate a cationic radical through an electron transfer (Eqs. (2) and (3)). The cationic dye radicals readily reacts with water or hydroxyl ions undergoing oxidation via or interacts effectively with $OH^\bullet$ species leading to the degradation of the dye (Eqs. (4) and (5)).

$$MB + h\nu(\text{vis}) \rightarrow MB^* \quad (1)$$

$$MB^* + O_2 \rightarrow MB + O_2 \quad (2)$$

$$MB^* \rightarrow MB^{\bullet +} + e^-(\text{aqueous}) \quad (3)$$

$$MB^{\bullet +} + OH^-(\text{or } H_2O) \rightarrow MB + OH^\bullet \quad (4)$$

$$MB + OH^\bullet \rightarrow \text{degradation} \quad (5)$$

For the mechanism of photosensitized oxidation, in presence of catalyst the excited state of MB inject an electron into the conduction band (Eq. (6)). Whereas, the dye is converted to the cationic dye radicals ($Dye^{\bullet +}$) that undergoes degradation to yield products as follows (Eqs. (7)–(10)) [49].

$$MB^* + TiO_2 \rightarrow MB^{\bullet +} + e^-_{CB}(TiO_2) \quad (6)$$

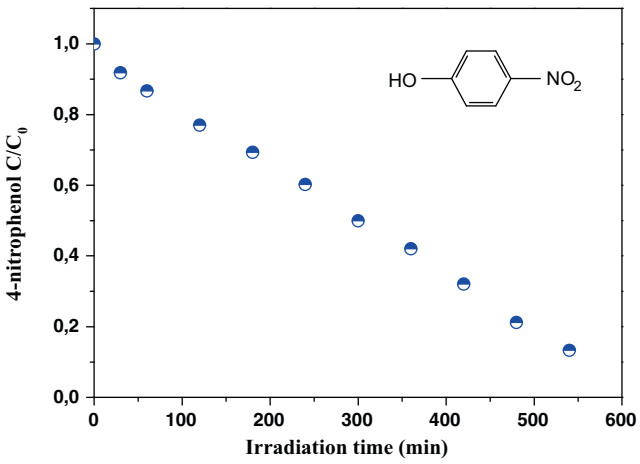

Fig. 11. Photocatalytic degradation of 4-nitrophenol (PNP) in aqueous suspension as a function of visible irradiation time using TiO_2(AC-700) (inset: molecular structure of PNP). Experimental condition: natural pH; C_0(PNP) = 30 ppm; m (catalyst) = 62.5 mg; V (solution) = 125 ml.

$$O_2 + e^- \rightarrow O^{\bullet}_2^- \quad (7)$$

$$MB^{\bullet+} + OH^- \rightarrow MB + OH^{\bullet} \quad (8)$$

$$MB^{\bullet+} + OH^{\bullet} \rightarrow \text{products} \quad (9)$$

$$MB^{\bullet+} + O^{\bullet}_2^- \rightarrow \text{products} \quad (10)$$

The photocatalytic process of TiO_2(AC-700) semi-conductor is confirmed by the degradation of 4-nitrophenol (PNP). Fig. 11 shows the photocatalytic results of PNP by TiO_2(AC-700). The total degradation rate of PNP was over 90% within 6 h of irradiation and the reaction follows first order kinetics with an apparent rate constant equal to 2.03×10^{-3} min^{-1}. PNP dissolved in water will form a colorless solution and this solution is very stable under light irradiation. Therefore, the degradation of PNP can be attributed only to the photocatalytic activity of TiO_2(AC-700). This experiment may prove that the TiO_2(AC-700) have the ability in the photocatalytic degradation process of MB under visible irradiation. Thus, the absorption of visible light by TiO_2(AC-700) produced hole in the valence band and electron in the conduction band. The electron–hole pairs, thus generated, are able of initiating oxidation and reduction reactions on the surface of TiO_2 particles. Holes (h^+_{VB}) react with adsorbed OH^- groups and produce $OH^{\bullet}$ radicals. Whereas, electrons (e^-_{CB}) react with O_2 and produce superoxide anion radical $O^{\bullet}_2^-$. $OH^{\bullet}$ and $O^{\bullet}_2^-$ radicals worked together to degrade MB.

The experimental results show that the degradation rate of MB using TiO_2(AC-700) is high compared to bare-TiO_2 and TiO_2-P25 which could be attributed to the anatase phase stability, the high surface area and the existence of SiO_2 oxides. As confirmed by many works, the rutile phase is generally less active due to lower surface affinity for many organic compounds and generally higher rates of recombination of photogenerated charge pairs. Moreover, the surface area which will help the adsorption of more dye molecules on the surface of catalyst and the band gap energy which may induce a modification in the valence band (VB) and conduction band (CB) levels causing higher CB and lower VB level. Thus the electron–hole recombination rate decreases during the illumination of catalyst [50–52].

Furthermore, the important factor which enhances the photoactivity of TiO_2 is the presence of SiO_2. Activated carbon impurities may improve the thermal stability of titania by suppressing the anatase-to-rutile phase transformation, the growth of crystalline size, the surface area and preserve a higher content of surface hydroxyl groups [37,53].

4. Conclusion

We reported the elaboration of TiO_2 through activated carbon addition with high stability and high activity under visible light. It was found that photoactivity of TiO_2 catalyst was improved by the addition of activated carbon. In fact, our results suggested that activated carbon matrix not only counterworked the growth of TiO_2 particles, prevented the agglomeration TiO_2 particles, retarded the transformation from anatase to rutile phase, but also the activated carbon produced a doping or/and junction effects by some structural AC mineral oxides, such oxide at least SiO_2.

The photocatalytic process and the photosensitized process were identified to contribute in the degradation process of MB under visible irradiation using TiO_2(AC-700), TiO_2 and P25. TiO_2(AC-700) shows higher degradation rate more than TiO_2 and TiO_2-P25 powders. Owing to its high performance in visible irradiation, the TiO_2(AC-700) solid prepared by sol–gel method is a very promising photocatalyst for the degradation of organic pollutants which must be tested under UV or solar irradiation.

References

[1] A. Fujishima, X. Zhang, Titanium dioxide photocatalysis: present situation and future approaches, Comptes Rendus Chimie 9 (2006) 750–760.
[2] J.M. Herrmann, Heterogeneous photocatalysis: fundamentals and applications to the removal of various types of aqueous pollutants, Catalysis Today 53 (1999) 115–129.
[3] H. Lachheb, E. Puzenat, A. Houas, M. Ksibi, E. Elaloui, C. Guillard, J.M. Herrmann, Photocatalytic degradation of various types of dyes (Alizarin S, Crocein Orange G, Methyl Red, Congo Red, Methylene Blue) in water by UV-irradiated titania, Applied Catalysis B: Environmental 39 (2002) 75–90.
[4] E. Bizani, K. Fytianos, I. Poulios, V. Tsiridis, Photocatalytic decolorization and degradation of dye solutions and wastewaters in the presence of titanium dioxide, Journal of Hazardous Materials 136 (2006) 85–94.
[5] K.H. Wang, Y.H. Hsieh, M.Y. Chou, C.Y. Chang, Photocatalytic degradation of 2-chloro and 2-nitrophenol by titanium dioxide suspensions in aqueous solution, Applied Catalysis B: Environmental 21 (1999) 1–8.
[6] L. Lhomme, S. Brosillon, D. Wolbert, J. Dussaud, Photocatalytic degradation of a phenylurea, chlortoluron, in water using an industrial titanium dioxide coated media, Applied Catalysis B: Environmental 61 (2005) 227–235.
[7] J Araña, J.M. Doña-Rodríguez, E. Tello Rendón, C. Garriga i Cabo, O. González-Díaz, J.A. Herrera-Melián, J. Pérez-Peña, G. Colón, NavíoF J.A., TiO_2 activation by using activated carbon as a support, Applied Catalysis B: Environmental 44 (2003) 161–172.
[8] H. Ibrahim, H. Lasa, Photo-catalytic conversion of air borne pollutants. Effect of catalyst type and loading in novel photo-CREC-air unit, Applied Catalysis B: Environmental 38 (2002) 201–213.
[9] C. Karunakaran, S. Senthilvelan, Fe_2O_3-photocatalysis with sunlight and UV light: oxidation of aniline, Electrochemistry Communications 8 (2006) 95–101.
[10] K. Melghit, A.K. Mohammed, I. Al-Amri, Chimie douce preparation, characterization and photocatalytic activity of nanocrystalline SnO_2, Materials Science and Engineering B 117 (2005) 302–306.
[11] A Martínez-de la Cruz, D. Sánchez Martínez, E. Loópez Cuéllar, Synthesis and characterization of WO_3 nanoparticles prepared by the precipitation method: evaluation of photocatalytic activity under vis-irradiation, Solid State Sciences 12 (2010) 88–94.
[12] A.M.T. Silva, C.G. Silva, G. Dražić, J.L. Faria, Ce-doped TiO_2 for photocatalytic degradation of chlorophenol, Catalysis Today 144 (2009) 13–18.
[13] Q. Chen, D. Jiang, W. Shi, D. Wu, Y. Xu, Visible-light-activated Ce–Si co-doped TiO_2 photocatalyst, Applied Surface Science 255 (2009) 7918–7924.
[14] J. Xu, Y. Ao, D. Fu, C. Yuan, A simple route for the preparation of Eu, N-codoped TiO_2 nanoparticles with enhanced visible light-induced photocatalytic activity, Journal of Colloid and Interface Science 328 (2008) 447–451.
[15] N. Takeda, T. Torimoto, S. Sampath, S. Kuwabata, H. Yoneyama, Effect of inert supports for titanium dioxide loading on enhancement of photodecomposition rate of gaseous propionaldehyde, Journal of Physical Chemistry 99 (1995) 9986–9991.
[16] N. Takeda, N. Iwata, T. Torimoto, H. Yoneyama, Influence of carbon black as an adsorbent used in TiO_2 photocatalyst films on photodegradation behaviors of propyzamide, Jouranl of Catalysis 177 (1998) 240–246.
[17] S. Fukahori, H. Ichiura, T. Kitaoka, H. Tanaka, Photocatalytic decomposition of bisphenol A in water using composite TiO_2–zeolite sheets prepared by a papermaking technique, Environmental Science Technology 37 (2003) 1048–1051.
[18] S. Fukahori, H. Ichiura, T. Kitaoka, H. Tanaka, Capturing of bisphenol A photodecomposition intermediates by composite TiO_2–zeolite sheets, Applied Catalysis B: Environmental 46 (2003) 453–462.
[19] M.C. Lu, J.N. Chen, K.T. Chang, Effect of adsorbents coated with titanium dioxide on the photocatalytic degradation of propoxur, Chemosphere 38 (1999) 617–627.

[20] S. Yamazaki, S. Matsunage, K. Hori, Photocatalytic degradation of trichloroethylene in water using TiO_2 pellets, Water Research 35 (2001) 1022–1028.
[21] M.V. Shankar, S. Anandan, N. Venkatachalam, B. Arabindoo, V. Murugesan, Fine route for an efficient removal of 2 4-dichlorophenoxyacetic acid (2,4-D) by zeolite-supported TiO_2, Chemosphere 63 (2006) 1014–1021.
[22] J. Marugá, D. Hufschmidt, M.J. López-Munõz, V. Selzer, D. Bahnemann, Photonic efficiency for methanol photooxidation and hydroxyl radical generation on silica-supported TiO_2 photocatalysts, Applied Catalysis B: Environmental 62 (2006) 201–207.
[23] X. Zhang, M. Zhou, L. Lei, Preparation of anatase TiO_2 supported on alumina by different metal organic chemical vapor deposition methods, Applied Catalysis A: General 282 (2005) 285–293.
[24] T. Yazawa, F. Machida, N. Kubo, T. Jin, Photocatalytic activity of transparent porous glass supported TiO_2, Ceramics International 35 (2009) 3321–3325.
[25] Y. Yu, J.C. Yu, J.G. Yu, Y.C. Kwok, Y.K. Che, J.C. Zhao, L. Ding, W.K. Ge, P.K. Wong, Enhancement of photocatalytic activity of mesoporous TiO_2 by using carbon nanotubes, Applied Catalysis A: General 289 (2005) 186–196.
[26] B. Tryba, A.W. Morawski, M. Inagaki, Application of TiO_2-mounted activated carbon to the removal of phenol from water, Applied Catalysis B: Environmental 41 (2003) 427–433.
[27] C.H. Ao, S.C. Lee, Enhancement effect of TiO_2 immobilized on activated carbon filter for the photodegradation of pollutants at typical indoor air level, Applied Catalysis B: Environmental 44 (2003) 191–205.
[28] C.H. Ao, S.C. Lee, Combination effect of activated carbon with TiO_2 for the photodegradation of binary pollutants at typical indoor air level, Journal of Photochemistry and Photobiology A: Chemistry 161 (2004) 131–140.
[29] S.X. Liu, X.Y. Chen, X. Chen, A TiO_2/AC composite photocatalyst with high activity and easy separation prepared by a hydrothermal method, Journal of Hazardous Materials 143 (2007) 257–263.
[30] J. Matos, J. Laine, J.-M. Herrmann, D. Uzcategui, J.L. Brito, Influence of activated carbon upon titania on aqueous photocatalytic consecutive runs of phenol photomineralization, Applied Catalysis B: Environmental 70 (2007) 461–469.
[31] J.-M. Herrmann, J. Matos, J. Disdier, C. Guillard, J. Laine, S. Malato, J. Blanco, Solar photocatalytic degradation of 4-chlorophenol using the synergistic effect between titania and activated carbon in aqueous suspension, Catalysis Today 54 (1999) 255–265.
[32] P. Periyat, K.V. Baiju, P. Mukundan, P.K. Pillai, K.G.K. Warrier, High temperature stable mesoporous anatase TiO_2 photocatalyst achieved by silica addition, Applied Catalysis A: General 349 (2008) 13–19.
[33] Patent, Monereau, Christian (FR), Moreau, Serge (FR) 2001, Improved activated carbon by acid treatment and its use in gas separation, Air Liquide (FR), EP1132341, http://www.freepatentsonline.com/EP1132341A1.html.
[34] H. Zhang, J.F. Banfield, Understanding polymorphic phase transformation behavior during growth of nanocrystalline aggregates: insights from TiO_2, Journal Physical Chemistry 104 (2000) 3481–3487.
[35] J.J. Li, J. Cui, N.Q. Zhao, C.S. Shi, X.W. Du, The properties of granular activated carbons prepared from fly ash using different methods, Carbon 44 (2006) 1298–1352.
[36] Y. Li, S. Zhang, Q. Yu, W. Yin, The effects of activated carbon supports on the structure and properties of TiO_2 nanoparticles prepared by a sol–gel method, Applied Surface Science 253 (2007) 9254–9258.
[37] X. Wang, Z. Hu, Y. Chen, G. Zhao, Y. Liu, Z. Wen, A novel approach towards high-performance composite photocatalyst of TiO_2 deposited on activated carbon, Applied Surface Science 255 (2009) 3953–3958.
[38] Y. Li, X. Li, J. Li, J. Yin, TiO_2-coated active carbon composites with increased photocatalytic activity prepared by a properly controlled sol–gel method, Materials Letters 59 (2005) 2659–2663.
[39] G.F.A. Kortum, Reflectance Spectroscopy: Principles, Methods, Applications, Springer-Verlag, New York, 1969.
[40] G Burgeth, H. Kisch, Photocatalytic and photoelectrochemical properties of titania-chloroplatinate(IV), Coordination Chemistry Reviews 230 (2002) 41–47.
[41] J.I. Pankov, Optical Processes in Semicondutors, Prentice-Hall Inc., New Jersey, 1996, 1971.
[42] K.Y. Jung, S.B. Park, S.K. Ihm, Local structure and photocatalytic activity of B_2O_3–SiO_2/TiO_2 ternary mixed oxides prepared by sol–gel method, Applied Catalysis B: Environmental 51 (2004) 239–245.
[43] R.V. Grieken, J. Aguado, M.J. López-Muñoz, J. Marugán, Synthesis of size-controlled silica-supported TiO_2 photocatalysts, Journal of Photochemistry Photobiology A: Chemistry 148 (2002) 315–322.
[44] T. Takagahara, K. Takeda, Theory of quantum confinement effect on excitons in quantum dots of indirect-gap materials, Physical Review 46 (1992) 15579–15583.
[45] S. Lagergren, About the theory of so-called adsorption of soluble substances, Kungliga Svenska Vetenskapsakademiens Handlingar 24 (1898) 1–39.
[46] H.B. Fu, C.S. Pan, W.Q. Yao, Y.F. Zhu, Visible-light-induced degradation of rhodamine B by nanosized Bi_2WO_6, Journal of Physical Chemistry B 109 (2005) 22432–22439.
[47] D. Chatterjee, A. Mahata, Visible light induced photodegradation of organic pollutants on dye adsorbed TiO_2 surface, Journal of Photochemistry and Photobiology A: Chemistry 153 (2002) 199–204.
[48] Y. Ma, J. Yao, Photodegradation of rhodamine B catalysed by TiO_2 thin films, Journal of Photochemistry and Photobiology A: Chemistry 116 (1998) 167–170.
[49] I.K. Konstantinou, T.A. Albanis, TiO_2-assisted photocatalytic degradation of azo dyes in aqueous solution: kinetic and mechanistic investigations a review, Applied Catalysis B: Environmental 49 (2004) 1–14.
[50] T. Sumita, T. Yamaki, S. Yamamoto, A. Miyashita, Photo-induced surface charge separation of highly oriented TiO_2 anatase and rutile thin films, Applied Surface Science 200 (2002) 21–26.
[51] K.V. Baiju, P. Periyat, P.K. Pillai, P. Mukundan, K.G.K. Warrier, W. Wunderlich, Enhanced photoactivity and anatase thermal stability of silica–alumina mixed oxide additives on sol–gel nanocrystalline titania, Materials Letters 61 (2007) 1751–1755.
[52] K.V. Baiju, P. Shajesh, W. Wunderlich, P. Mukundan, S. Rajesh Kumar, K.G.K. Warrier, Effect of tantalum addition on anatase phase stability and photoactivity of aqueous sol–gel derived mesoporous titania, Journal of Molecular Catalysis A: Chemical 276 (2007) 41–46.
[53] L. Sikong, J. Damchan, K. Kooptarnond, S. Niyomwas, Effect of doped SiO_2 and calcinations temperature on phase transformation of TiO_2 photocatalyst prepared by sol–gel method, Songklanakarin Journal of Science and Technology 30 (2008) 385–391.